Prepulse effect on intense femtosecond laser pulse propagation in gas

Antonio Giulietti, Paolo Tomassini, Marco Galimberti, Danilo Giulietti,[a] Leonida A. Gizzi, Petra Koester, and Luca Labate[b]
Intense Laser Irradiation Laboratory, IPCF-CNR, via Moruzzi, 1 56124 Pisa, Italy

Tiberio Ceccotti, Pascal D'Oliveira, Thierry Auguste, Pascal Monot, and Philippe Martin
CEA-DSM/DRECAM/SPAM, Gif sur Yvette Cedex, France

(Received 1 June 2006; accepted 9 August 2006; published online 15 September 2006; publisher error corrected 21 February 2007)

The propagation of an ultrashort laser pulse can be affected by the light reaching the medium before the pulse. This can cause a serious drawback to possible applications. The propagation in He of an intense 60-fs pulse delivered by a Ti:sapphire laser in the chirped pulse amplification (CPA) mode has been investigated in conditions of interest for laser-plasma acceleration of electrons. The effects of both nanosecond amplified spontaneous emission and picosecond pedestals have been clearly identified. There is evidence that such effects are basically of refractive nature and that they are not detrimental for the propagation of a CPA pulse focused to moderately relativistic intensity. The observations are fully consistent with numerical simulations and can contribute to the search of a stable regime for laser acceleration. © *2006 American Institute of Physics*.
[DOI: 10.1063/1.2351961]

I. INTRODUCTION

The achievement of conditions for stable and reproducible propagation of powerful ultrashort pulses in gases and plasmas is a key issue for many applications, including fast ignition of inertial confinement fusion (ICF) compressed fuel and particle acceleration by plasma electron waves. Particularly in this latter case, though extremely promising results have been obtained in the last few years,[1–4] there is still a lack of reproducibility due to the poor knowledge and control of a number of instabilities occurring during the propagation of the ultrashort laser pulse in the gas/plasma medium where the electron waves are generated. This fact results in a poor shot-to-shot reproducibility of the energy and energy spread of the produced electron bunches, as well as in a considerable variation of the angular distribution (collimation) and direction of emission of such bunches. Most of the propagation instabilities, including filamentation and hosing,[5,6] are expected and have proved to increase their detrimental effect by increasing the intensity of the focused laser pulse. It seems then reasonable for the transition from acceleration experiments to practical and reliable "table-top" accelerators, to consider laser pulses of not extreme intensity propagating towards long acceleration paths, possibly in a guided mode.[7] The ultrashort (typically tens of femtosecond) pulses are usually generated by the chirped pulse amplification (CPA) technique. At the output of a CPA laser, the main high power femtosecond pulse is accompanied by a nanosecond "pedestal" due to the amplified spontaneous emission (ASE), and a picosecond pedestal due to the unavoidable limit in the compression of the chirped pulse. The contrast ratios between the femtosecond peak power and the power of the two precursors are typically of the order of 10^6 for the ASE and 10^3 for the picosecond pedestal. Some very effective methods of increasing the contrast of one or both the two pedestals have been successfully implemented so far. Recently, the contrast has been greatly improved with a "plasma mirror" technique.[8] However, the levels of contrast ratio mentioned above are still the reference ones for most of the laser systems operating at high repetition rates, as requested for practical accelerators. Further, it has to be said that, at least for the case of the ASE pedestal, some successful attempts in using such an early emission to create a preformed plasma suitable for optimizing the acceleration process have been done, both in the case of thin foils targets[9] and for the creation of plasma channels in gases to be used either as optical guides for the CPA pulse[1,10] or to optimize the injection of fast electrons in the laser wake behind the pulse.[11]

In this paper we report and discuss the main results of an experiment of propagation of a CPA pulse of moderately relativistic intensity in gas: the experiment was particularly devoted to evidence the effects of the precursor pedestals of the main pulse. The experiment was performed by focusing the laser pulse in a gas jet. Since our purpose was only to study propagation, a subsonic gas jet was used and the pulse was focused in its center, different from most acceleration experiments in which supersonic gas jets are used and the pulse is focused at the high density gradient of the gas boundary.

In the next section the experimental method and setup are briefly described. Section III is devoted to the presentation of the experimental data, including the electron density distribution produced by the gas ionization during the propagation of the ultrashort pulse together with its precursors. The electron density maps reveal for the first time details of great interest, thanks to the high quality interferograms and the original algorithm for their deconvolution. The interferometric data are then correlated with imaging and spectros-

[a]Also at Dip. Fisica, Università di Pisa and INFN.
[b]Also at Laboratori Nazionali di Frascati, INFN.

copy data of the laser pulse transmitted after propagation. The most relevant physical features are then discussed in Sec. IV. with the help of data obtained from a numerical code that simulates the laser pulse propagation self-consistently with the ionization of the gas.

II. THE EXPERIMENT

The experiment was performed at the SLIC laser facility in the Saclay Centre of CEA (France) with the 10 Terawatt UHI10 laser system, delivering 60-fs, linearly polarized, laser pulses at 800 nm from a Ti:Sa system operating in the CPA mode. The precursors of the main pulse were carefully monitored by a third-order cross-correlator,[12] supplying both the nanosecond and picosecond scale contrast of the pulse. The ASE was found to last about 1 ns before the main pulse with a contrast ratio of $\approx 10^6$, while the picosecond *pedestal* of the femtosecond pulse had a contrast ratio between 10^4 and 10^3. The propagation was studied by focusing with an $f/5$ off-axis parabola, in a helium gas jet (500 μm from the nozzle), the laser pulse at a nominal intensity of 3×10^{18} W cm^{-2}, corresponding to a moderately relativistic field of normalized parameter $a_o = 1.2$. The focus of the ASE was found not to lie in the same position as the focus of the CPA pulse, this latter being located about 400 μm toward the laser. The laser spot (13 μm full width at half-maximum (FWHM), $M^2 = 3.3$) was imaged from the transmitted light with an $f/5$ lens on a CCD camera to get its intensity distribution. The spectrum of the transmitted laser pulse was also obtained from the light collected by the same $f/5$ optics and analyzed by a grating spectrometer whose nominal resolution was 0.5 nm. The gas jet was a subsonic flow of He from a nozzle with a rectangular (slit) output 3×0.3 mm in size. Gas jets of this kind were already carefully characterized.[13] The laser beam axis was set to be in the longitudinal symmetry plane of the gas jet. A fraction of the femtosecond pulse was doubled in frequency and used as an optical probe perpendicular to both the main pulse propagation axis and the gas flow axis. The frequency duplication was obtained with a KDP-Type-I, 2-mm-thick crystal: the duration of the probe pulse after duplication was numerically estimated to be $\leqslant 120$ fs. The probe pulse was timed with respect to the main CPA pulse by means of an optical delay. High quality interferograms were obtained in a Mach-Zehnder configuration.[14] Reproducible series of interferograms taken at different delays showed the evolution of the gas ionization within steps of few hundreds of femtoseconds during the laser pulse propagation. Below, we will show two of such interferograms [Figs. 1(a) and 1(b)], one before and one after the CPA pulse passed through the focal region, respectively. A third interferogram (Fig. 2) is also shown; it was obtained in conditions similar to the first one, but in a configuration allowing higher magnification. The arrival of the CPA pulse in the nominal position of the focus was timed with an accuracy comparable to the probe pulse duration. Due to the low refractive index of He and the small transverse thickness of the gas layer (300 μm), the density of the neutral gas in the region of propagation could not be measured. It can be nevertheless roughly inferred from the maximum electron

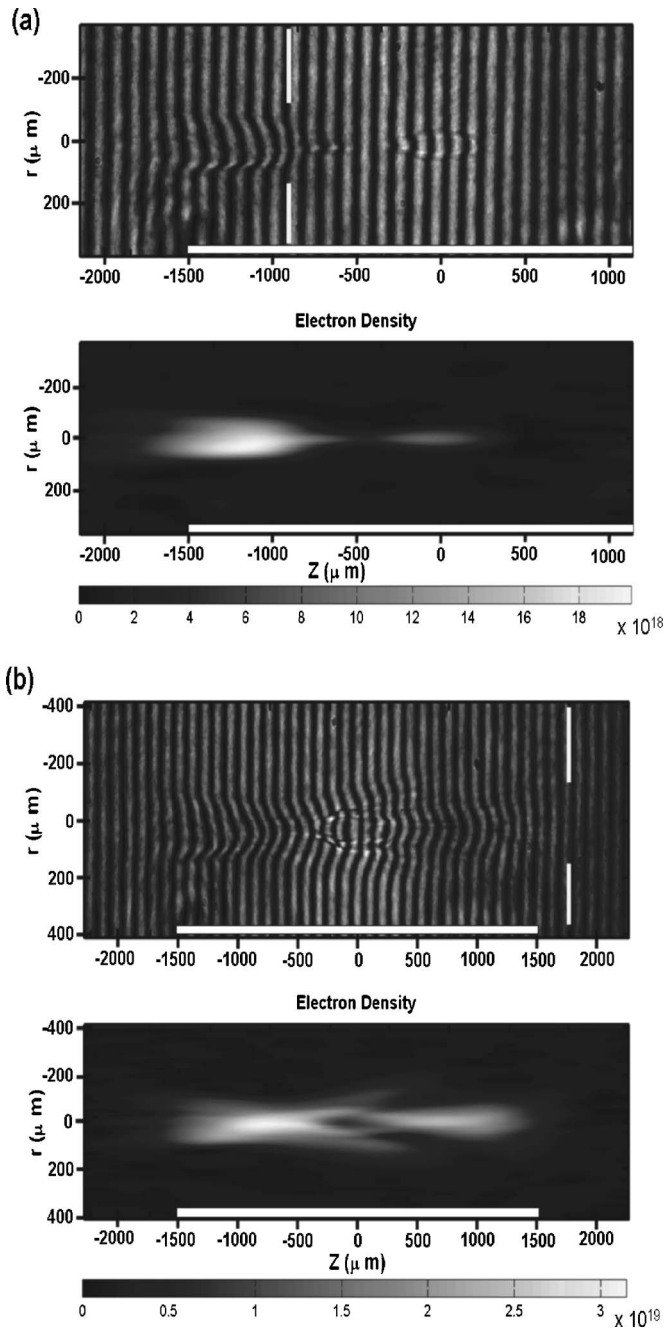

FIG. 1. Data from optical probing. (a) Data taken 3 ps before the CPA pulse reached the nominal focus. (b) Data taken 6 ps after the CPA pulse passed through the nominal focus. Top pictures: interferograms. Bottom pictures: retrieved electron density distributions. The laser pulse is coming from left; the gas is flowing from bottom.

density measured in the plasma totally ionized by the powerful CPA pulse. In this way we found that the He density was of the order of 10^{19} at./cm^3 on the axis of propagation. Such a density definitely is in the range of interest for electron acceleration by plasma waves generated with ultrashort laser pulses. As the CPA pulse propagated perpendicularly to the gas flow, there was a significant density gradient along the flow in the ionized region. The maximum electron density in the ionized region was measured at about 70 μm from the axis (≈ 430 μm from the nozzle). We could thus infer that the maximum density involved in the ionization process

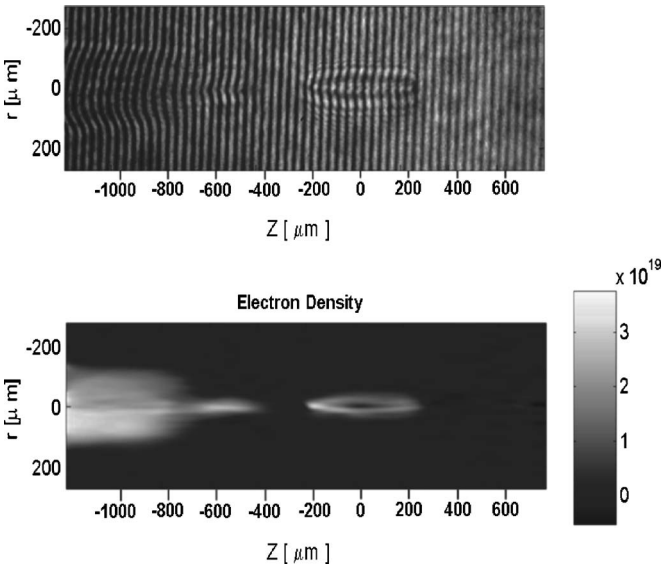

FIG. 2. Data from optical probing. Top: interferogram obtained in condition similar to Fig. 1(a) but with a magnifying optics. Bottom: the retrieved electron density distribution. The laser pulse is coming from left; the gas is flowing from bottom; fringes are moved in the opposite direction with respect to Fig. 1.

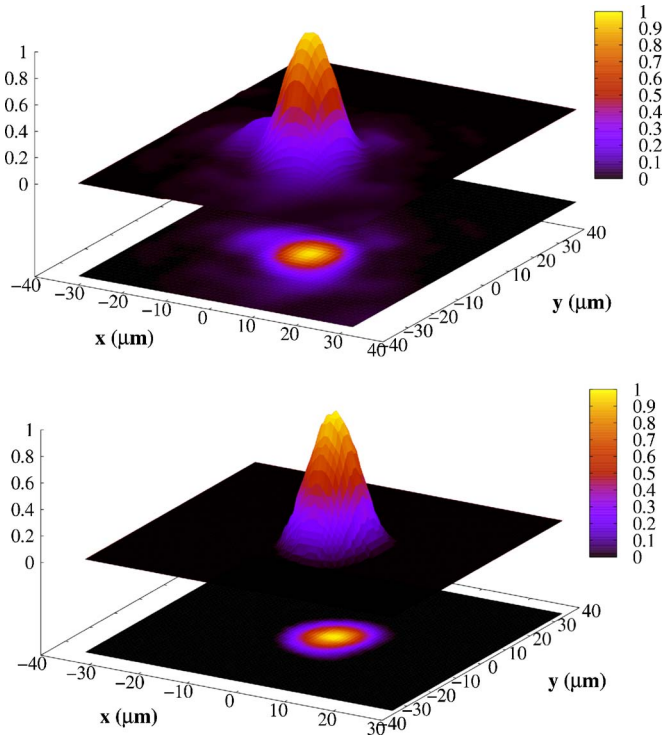

FIG. 3. Intensity distribution in the far field of the laser obtained from the transmitted light with an *f*/5 imaging optics. Top: after propagation in vacuum. Bottom: after propagation in He. The two plots are not to scale with respect to one another.

was about 1.5×10^{19} at./cm^3. The optical breakdown threshold[15] at this He density for nanosecond laser pulses (the ASE pedestal in our case) can be estimated of about 2×10^{12} W cm^{-2}. With the contrast ratio of 10^6 we had, the ASE intensity was just above threshold, and in fact we observed a reproducible early plasma formation due to ASE at this He density. It is interesting to note that at a slightly reduced He density (30%–40% lower), the ASE intensity drops below the breakdown threshold. As a matter of fact, we did not observe experimentally any preformed plasma at this reduced He density.

III. THE EXPERIMENTAL DATA

Figure 1 shows two interferograms taken during the propagation of the CPA pulse through the gas jet. The corresponding electron density distribution is also shown. This latter has been obtained by extracting the phase-difference map with a specialized Continuous Wavelet Transform Ridge Extraction code.[16] This technique is able to evidence local variations of phase better than other techniques based on fast Fourier transforms. The phase-difference map was then processed with a generalized ABEL inversion algorithm,[17] in which the usual axial symmetry requirement is partially relaxed by means of a truncated Legendre polynomial expansion in the azimuthal angle. This novel inversion algorithm can deal with moderately asymmetrical phase-shift maps without introducing artifacts in the plasma density map. The laser pulse was coming from the left-hand side. The horizontal white bar defines the position of the 3-mm slit nozzle of the He jet (z=0 is its center); the vertical bars mark the position of the CPA pulse. Notice that the pulse path in the gas is longer than 3 mm, due to the lateral expansion of the He jet.[10,13] The interferogram of Fig. 1(a) was taken 3 ps before the CPA pulse reached the nominal focus. Let us consider the corresponding electron density distribution: at the center of the gas jet (z=0) there is a preformed plasma created by the ASE hundreds of picoseconds before the arrival of the CPA pulse; this plasma has already expanded and the analysis of more magnified patterns (see Fig. 2) shows that its density has a minimum on the axis, due to the hydrodynamic expansion of the hot plasma in the surrounding cold gas. Between the ASE preformed plasma and the front of the CPA pulse coming from the left, a filament of plasma of length of the order of 300 to 500 μm and diameter of $\approx$20 μm is visible. This is due to the ionization of the gas produced by the most intense part of the picosecond pedestal, starting about 1 ps before the CPA pulse. At that time, the pedestal intensity in that region close to the waist is able to ionize the gas, as also proved by the numerical simulation showed in the next section. Actually, the pedestal is just above the intensity requested for the ionization. For this reason, at a given probe delay, the electron density can show a minimum just before the front of the ultraintense pulse, where both picosecond and femtosecond pulses are slightly defocused, and their intensity decreases, with consequent lower level of ionization for the picosecond pedestal and a sudden rise of full ionization due to the femtosecond pulse with its intensity three orders of magnitude larger. This density minimum is clearly visible both in the magnified interferogram of Fig. 2 and in the simulation (Fig. 5).

On the left of the CPA pulse front, the ionized region has a radius of about 100 μm, since the intensity needed for ionizing the gas is reached transversally at that distance from the axis. All these features are well reproduced by the nu-

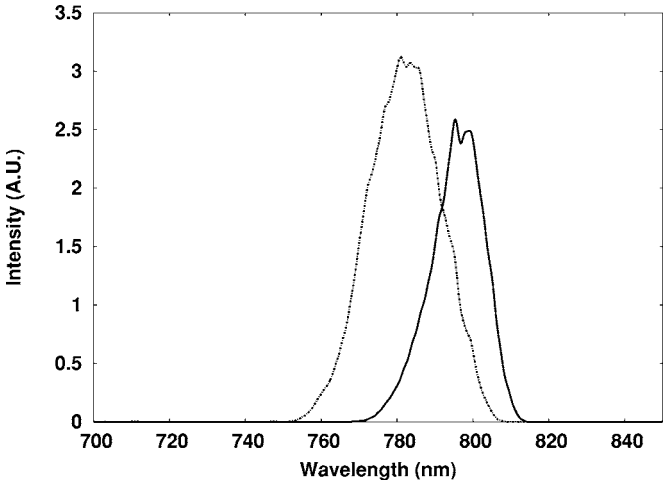

FIG. 4. Spectra of the transmitted laser light after (solid line) propagation in vacuum and (dotted line) propagation in He. The two spectra are not to scale with respect to one another.

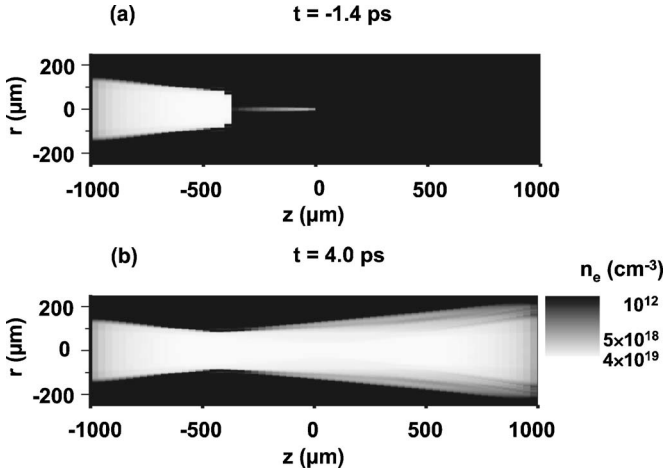

FIG. 5. Data from numerical simulation showing the electron density distribution during the propagation (from left) of the CPA pulse preceded by the picosecond pedestal (a) and after leaving the focal region (b). Contrast ratio 10^4. The snapshots show the central 2-mm portion (±1 mm around the focus) of the pulse path in the He jet.

merical simulation, as we will see later. The interferogram of Fig. 1(b) was taken 6 ps after the CPA pulse passed through the nominal focus, when the pulse itself is leaving the gas. The main feature to be noticed is the splitting of the CPA pulse front in two parts as a consequence of its interaction with the hollow plasma (visible in the electron density map) preformed by the ASE in the focus. This splitting process results in a central part and an external ring diverging at angles larger than the focusing angle. The central part of the pulse can be observed indirectly here from the central feature of the electron density beyond (right-hand side of) the preformed plasma, but it is directly observable in the image of the laser spot in Fig. 3 (bottom). In fact, Fig. 3 shows the intensity distribution in the laser far-field spot imaged from the transmitted light by an optics of the same aperture as the focusing optics ($f/5$). In the picture on top, taken in vacuum, we just see the distribution of the original laser spot, with a small but sensible amount of aberration. Rather surprisingly, these aberrations are cancelled out in the spot imaged after propagation in helium (bottom of Fig. 2) in the same conditions of the interferograms of Fig. 1. In fact, the interaction of the CPA pulse with the hollow plasma preformed by the ASE, results in a spatial filtering of the pulse itself, as indirectly observed from the electron density distribution of Fig. 1(b). Only the central part of the spot is collected by the imaging optics, while the marginal part (the external ring), more aberrated, is scattered to larger angles. A similar space filtering of the pulse had been observed in quite different conditions, namely the propagation of a femtosecond pulse through an overcritical thin plasma produced by ultrafast ionization.[18] In addition, the spectra were obtained from the light transmitted forward and collected with the same $f/5$ optics as for the images of the spot in Fig. 3 (bottom). Figure 4 shows two spectra: one after propagation in vacuum (solid line), i.e., the original laser spectrum; the other (dotted line) is the spectrum after propagation in the same conditions of the interferograms of Fig. 1 and spot image of Fig. 3 (bottom). We can see that propagation in the gas and consequent ionization produce a net blue shift and a moderate broadening of the pulse. The mean spectral values calculated for the transmitted light over 27 shots, are as follows: shift $\delta\lambda = 15.0 \pm 2.6$ nm and bandwidth $\Delta\lambda = 50 \pm 7$ nm.

IV. SIMULATIONS AND DISCUSSION

The numerical code used to simulate the laser propagation through the gas jet and the electron density distribution resulting from the interaction is based on the solution of the standard paraxial wave equation in cylindrical geometry. In the frame moving with the pulse, the equation of propagation for the slowly varying complex amplitude of the linearly polarized laser field $E(r,z,t)$ is as follows:

$$\frac{\partial E(r,z,t)}{\partial z} - \frac{i}{2k_0}\nabla_\perp^2 E(r,z,t) + \frac{i\Delta}{2c^2k_0}E(r,z,t) = 0,$$

where

$$\nabla_\perp^2 = \frac{1}{r}\frac{\partial}{\partial r}\left(r\frac{\partial}{\partial r}\right)$$

is the transverse Laplacian operator in cylindrical geometry, c is the speed of light, and k_0 is the vacuum wave number. Δ takes into account the nonlinear response of the plasma, which is treated in the quasi-static approximation. This consists in neglecting the time-derivatives in the plasma response. This approximation is valid for pulse lengths longer than the plasma period ($\tau \gg \omega_p^{-1}$), which is the case here. Δ takes the form[18]

$$\Delta = \max\left[0, \omega_{p0}^2\left(\frac{1}{\langle\gamma\rangle} - 1\right) + c^2\nabla_\perp\left(\frac{\nabla_\perp\langle\gamma\rangle}{\langle\gamma\rangle}\right) + c^2\frac{\nabla_\perp\langle\gamma\rangle\nabla_\perp n_{e0}}{n_{e0}(0)}\right],$$

where ω_{p0} is the undisturbed plasma frequency, and $n_{e0}(r,z)$ is the space-varying electron density, produced by the picosecond rising front of the pulse, prior to the interaction with the high-intensity part of the laser pulse. $n_{e0}(0)$ is the on-axis

(in $r=0$) density. As in previous work,[19–22] we treat electron cavitation by setting $\Delta=\max[0,\Delta]$, in order to cure unphysical effects ($n_e<0$) in the case of complete cavitation. $\langle\gamma\rangle$ is the optical-cycle averaged relativistic factor where the brackets stand for the cycle average. $\langle\gamma\rangle$ is given by

$$\langle\gamma\rangle=\sqrt{1+\frac{E^2}{2E_c^2}}.$$

$E_c=m_{e0}\omega_0 c/e$ is the Compton field, with m_{e0} and e the electron rest mass and charge, respectively, and ω_0 the laser frequency.

The equation of propagation is solved iteratively, and self-consistently with the ionization rate equations, on a (r,z) grid using a standard finite element method. The field ionization is described either by Ammosov-Delone-Krainov tunneling model[23] or by Perelomov-Popov-Terent'ev formula,[24–27] the latter being valid in both multiphoton and tunneling regimes of ionization. The results were found not to be sensitive to the different ionization rates. We assume a Gaussian spatial laser profile at the entrance of the gas jet with peak power and time profile consistent with the experimental conditions. In particular, the pulse shape used in the simulations is a fit by two Gaussians of a third-order correlation trace given in Ref. 12. The jet has a trapezoidal profile along the direction of propagation with a 1.5-mm plateau (±750 μm on each side of the vacuum focus position) and 250-μm gradients, and is Gaussian in the transverse direction, with a 500 μm FWHM. The ASE was not included in the simulation.

The simulation shows that the picosecond pedestal starts to ionize 2.7 ps before the femtosecond pulse reaches the nominal focus; i.e., the middle of the jet. The He preplasma produced in this way is a singly ionized plasma, 20 μm in diameter and 300 μm in length. As expected, we observe that the propagation of the picosecond pedestal is dominated by refraction. In this regime of interaction ($a\ll 1$), only the Kerr effect in the neutral gas could lead to nonlinear effects, but the length of the medium is too small, and the density as well, as the nonlinear index of refraction of He ($n_2\sim 10^{-28}$ cm^2/W) is too low. Moreover, self-focusing by the Kerr effect stops once the ionization of the medium starts. All these features are in excellent agreement with the experimental data [see data in Fig. 1(a)]. From the simulation data on the pulse intensity distribution during the propagation (not shown in this paper) we find that the subsequent propagation of the CPA pulse is weakly disturbed by ionization-induced refraction. Only the rising edge of the pulse and the wings of the beam are concerned. We do not observe in the simulation any significant increase of the intensity due to relativistic self-focusing. This point agrees with the experimental images of the spot after propagation, whose size is basically the same as the spot size in vacuum. The simulation shows that the He jet is doubly ionized on its entire length, and the radius of the plasma is about 100 μm. Again, all these features fully agree with the experimental data.

It is interesting to compare the experimental electron density maps of Figs. 1 and 2 with the corresponding maps obtained from the simulation. Preliminarily, we notice that the numerical code includes ionization and accounts for the first and second ionization stages of helium. To this respect, we compare the simulation data with the experimental ones on the basis of the estimation we did, starting from the maximum electron density we observed in the region ionized by the main pulse. We reasonably assume that this density correspond to the doubly ionized He.

Figure 5 shows two snapshots from the numerical simulation of the electron density distribution after the propagation (from left) of the CPA pulse preceded by the picosecond pedestal with a contrast ratio of 10^4. Figures 5(a) and 5(b) can be compared with Figs. 1(a) and 1(b), respectively. We have to take into account that the ASE is not included in the simulation: consequently there is no preformed plasma, nor interaction of CPA pulse with it. Considering this point, the basic features of the experimental density maps are reproduced by simulation, including the early ionization produced by the picosecond precursor in a narrow filament behind the CPA pulse. In addition, the location and size of the regions where He is almost totally ionized are reproduced, as well as for the regions singly ionized.

Three apparent discrepancies can be explained. First, Fig. 5(a) gives an electron density map consistent with the map of Fig. 1(a) but 1.6 ps later (−1.4 ps in place of −3.0 ps). The reason is that, while $z=0$ is the center of the gas jet for both simulated and experimental maps, in the meantime, $z=0$ is (i) the focus of the CPA pulse in the simulation, but (ii) the focus of the ASE in the experimental maps. Now, we know (see Sec. II) that the CPA pulse focuses at about −400 μm with respect to the ASE, which roughly corresponds to the difference above.

Second, the ionization front of the CPA pulse, as shown by the simulation snapshot of Fig. 5(a) is very sharp, as expected from a few-cycle ionization at intensities of the order of 10^{18} W/cm^2. On the contrary, the density maps obtained from the interferograms [see Fig. 1(a) or, in more detail in Fig. 2] show a smooth ionization front with a density gradient of the order of 100 μm. This seems definitely not consistent with ultrafast ionization. This puzzling paradox has been recently solved.[28] It has been proved that the smooth gradient is not real, but is a consequence of the finite transit time of the probe through the ionized region whose front moves at the speed of light.

Third, the simulation does not reproduce a weak asymmetry in the radial density distribution, which is observable in the interferograms of Figs. 1 and 2. The electron density appears to be higher on bottom (positive r) than on top (positive r) of the interferograms. This asymmetry is real and due to the density gradient of the gas, which is flowing from the bottom. Since this aspect is not essential for the propagation along the axis ($r=0$), the simulation considered a gas density distribution uniform along r.

For what concerns the blueshift of the transmitted pulse, it can be produced only when the CPA pulse, including its wings, propagates at moderate intensities, not far from the ionization threshold. In our experiment this low level of in-

tensity occurs either (a) in the pulse marginal wings, which are, however, scattered out by the interaction with the preformed plasma, as proved by the previous data, and do not contribute to the spectrum of Fig. 4 or (b) in the early or late propagation of the pulse (e.g., at 1 mm from the focus the intensity is more than two orders of magnitude lower than in the focus itself). We can tentatively conclude that the blueshift we observe is produced during its early and late propagation of the pulse, when it is only partially focused, at an intensity making the ionization process as long as the pulse duration. As a matter of fact, the simulation reproduces a blueshift, whose value is comparable with the experimental value, but the simulated shift depends on the density profile of the gas. Since the actual density profile is not known, a quantitative comparison between the experimental and simulated shift was not possible.

In conclusion, we have obtained relevant data on the propagation of a fairly relativistic ultrashort CPA laser pulse in gas, in conditions of interest for acceleration of electrons in plasmas. Time- and space-resolved measurements of the free electron density revealed novel features on the early ionization produced by the precursors of the CPA pulse; namely, the ASE and the picosecond pedestal. These data, combined with far-field imaging and spectroscopy of the transmitted pulse, show that, at this level of intensity, the propagation of the CPA pulse is stable and reproducible, only marginally affected by moderate refraction effects. This general conclusion is fully confirmed by the numerical simulation, together with most of the features observed experimentally. The spectrum of the pulse after propagation resulted slightly blueshifted and broadened. These findings encourage to further investigate this regime of propagation over longer gas paths, as required for an efficient and stable class of new "table-top" laser driven accelerators.

ACKNOWLEDGMENTS

Authors are grateful to the SLIC scientific and technical staff. The collaborative work of the ILIL team (from CNR, Pisa-Italy) with the PHI team (CEA, Saclay-France) was supported by the EU scheme for the access to large facilities within the LASERNET network.

This work was also partially supported by INFN-Italy within the project PLASMONX. One of the authors (M.G.) is presently supported with a research contract funded by the Italian Ministry for Education, University and Research within the project BLISS on laser fusion. Last but not least, the authors greatly acknowledge the significant contribution of Andrea Gamucci to the editing of the manuscript.

[1] T. Hosokai, K. Kinoshita, T. Ohkubo *et al.*, Phys. Rev. E **73**, 036407 (2006).
[2] S. P. D. Mangles, C. D. Murphy, and Z. Najmudin, Nature (London) **431**, 535 (2004).
[3] C. G. R. Gedds, Cs. Toth, and J. van Tilborg, Nature (London) **431**, 538 (2004).
[4] J. Faure, Y. Glinec, and A. Pukhov, Nature (London) **431**, 541 (2004).
[5] Z. Najmudin, K. Krushelnik, E. L. Clark *et al.*, CLF Annual Report 1998/99, Rutherford Appleton Laboratory (U.K.) RAL-TR-1999–062, p. 18 (1999).
[6] B. J. Duda, R. G. Hemker, K. C. Tzeng, and W. B. Mo, Phys. Rev. Lett. **83**, 1978 (1999).
[7] H. Sheng, K. Y. Kim, V. Kumarappan, B. D. Layer, and H. M. Milchberg, Phys. Rev. E **72**, 036411 (2005).
[8] G. Doumy, F. Quere, O. Gobert, M. Perdrix, Ph. Martin, P. Audebert, J. C. Gauthier, J.-P. Geindre, and T. Wittmann, Phys. Rev. E **69**, 026402 (2004).
[9] D. Giulietti, M. Galimberti, A. Giulietti, L. A. Gizzi, P. Tomassini, M. Borghesi, V. Malka, S. Fritzler, M. Pittman, and K. Taphouc, Phys. Plasmas **9**, 3655 (2002).
[10] A. Gamucci, M. Galimberti, D. Giulietti, L. A. Gizzi, L. Labate, C. Petcu, P. Tomassini, and A. Giulietti, Appl. Phys. B: Lasers Opt. doi: 10.1007/s00340-006-2268-0 (2006).
[11] T. Hosokai, K. Kinoshita, A. Zhidkov, K. Nakamura, H. Kotaki, M. Kando, K. Nakajima, and M. Uesaka, Phys. Plasmas **11**, L57 (2004).
[12] P. D'Oliveira, S. Dobosz, S. Hulin, P. Monot, F. Reau, and T. Auguste, J. Opt. Soc. Am. B **19**, 2603 (2002).
[13] T. Auguste, M. Bougeard, E. Caprin, P. D'Oliveira, and P. Monot, Rev. Sci. Instrum. **70**, 2349 (1999).
[14] S. Dobosz, P. D'Oliveira, S. Hulin, P. Monot, F. Reau, and T. Auguste, Phys. Rev. E **65**, 047403 (2002).
[15] G. V. Ostrovskaya and A. N. Zaidel', Sov. Phys. Usp. **16**, 834 (1974).
[16] P. Tomassini, A. Giulietti, L. A. Gizzi, M. Galimberti, D. Giulietti, M. Borghesi, and O. Willi, Appl. Opt. **40**, 6561 (2001).
[17] P. Tomassini and A. Giulietti, Opt. Commun. **199**, 143 (2001).
[18] D. Giulietti, L. A. Gizzi, A. Giulietti, A. Macchi, D. Teychenné, P. Chessa, A. Rousse, G. Cheriaux, J. P. Chambaret, and G. Darpentigny, Phys. Rev. Lett. **79**, 3194 (1997).
[19] H. S. Brandi, C. Manus, G. Mainfray, and T. Lehner, Phys. Rev. E **47**, 3780 (1993).
[20] G. Z. Sun, E. Ott, Y. C. Lee, and P. Guzdar, Phys. Fluids **30**, 526 (1987).
[21] A. B. Borisov, A. V. Borovskiy, V. V. Korobkin, A. M. Prokhorov, C. K. Rhodes, and O. B. Shiryae, Phys. Rev. Lett. **65**, 1753 (1990).
[22] G. Bannaud, H. S. Brandi, C. Manus, G. Mainfray, and T. Lehner, Phys. Plasmas **1**, 968 (1994).
[23] P. Gibbon, P. Monot, R. Auguste, and G. Mainfray, Phys. Plasmas **2**, 1305 (1995).
[24] M. V. Ammosov, M. B. Delone, and V. P. Kraïnov, Sov. Phys. JETP **64**, 1191 (1986).
[25] A. M. Perelomov, V. S. Popov, and M. V. Terent'ev, Sov. Phys. JETP **23**, 924 (1966).
[26] A. M. Perelomov, V. S. Popov, and M. V. Terent'ev, Sov. Phys. JETP **24**, 207 (1967).
[27] A. M. Perelomov and V. S. Popov, Sov. Phys. JETP **25**, 336 (1967).
[28] M. Galimberti, J. Opt. Soc. Am. A (to be published).